

Article

The Reliability of SAC305 Individual Solder Joints during Creep–Fatigue Conditions at Room Temperature

Mohammed Abueed ^{1,*}, Raed Al Athamneh ², Moayad Tanash ² and Sa'd Hamasha ³¹ Department of TD ATA Automation, Intel Corporation, Hillsboro, OR 97124, USA² Department of Industrial Engineering, Faculty of Engineering, The Hashemite University, Zarqa 13133, Jordan³ Department of Industrial and Systems Engineering, Samuel Ginn College of Engineering, Auburn University, Auburn, AL 36849, USA

* Correspondence: mohammed.abueed@intel.com

Abstract: The failure of one solder joint out of the hundreds of joints in a system compromises the reliability of the electronics assembly. Thermal cycling is a result of both creep–fatigue mechanisms working together. To better understand the failure process in thermal cycling, it is crucial to analyze both the effects of creep and fatigue mechanisms in a methodical manner. In this work, individual solder junctions are subjected to accelerated shear fatigue testing to investigate the effects of creep and fatigue on joint dependability at room temperature. A modified fixture is used to conduct fatigue tests on an Instron 5948 micromechanical tester. SAC305 joints with an OSP surface finish were cycled under stress control at first, and then the strain was maintained for a set amount of time. In this investigation, three stress amplitudes of 16, 20, and 24 MPa are used, together with varying residence periods of 0, 10, 60, and 180 s. The fatigue life of solder junctions is described for each testing condition using the two-parameter Weibull distribution. Additionally, as a function of stress amplitude and residence time, a dependability model is created. For each testing scenario, the progression of the stress–strain loops was studied. By quantifying relevant damage metrics, such as plastic work per cycle and plastic strain at various testing circumstances, the damage due to fatigue is distinguished from creep. To investigate the relationships between plastic work and plastic strain with fatigue life, the Coffin–Manson and Morrow Energy model is used. The results indicate that using greater stress magnitudes or longer dwell periods significantly shortens fatigue life and dramatically increases plastic work and plastic strain. The housing impact is significant; in some circumstances, testing with a longer dwelling period and lower stress amplitude resulted in more damage than testing with a shorter dwelling period and higher stress levels. When illustrating the fatigue behavior of solder junctions under various stress amplitudes or dwellings, the Coffin–Manson and Morrow Energy model were both useful. In the end, general reliability models are developed as functions of plastic work and plastic strain.



Citation: Abueed, M.; Al Athamneh, R.; Tanash, M.; Hamasha, S. The Reliability of SAC305 Individual Solder Joints during Creep–Fatigue Conditions at Room Temperature. *Crystals* **2022**, *12*, 1306. <https://doi.org/10.3390/cryst12091306>

Academic Editors: Ulrich Prael, Sergey Guk and Faisal Qayyum

Received: 15 August 2022

Accepted: 12 September 2022

Published: 15 September 2022

Publisher's Note: MDPI stays neutral with regard to jurisdictional claims in published maps and institutional affiliations.



Copyright: © 2022 by the authors. Licensee MDPI, Basel, Switzerland. This article is an open access article distributed under the terms and conditions of the Creative Commons Attribution (CC BY) license (<https://creativecommons.org/licenses/by/4.0/>).

Keywords: solder joints; lead-free; reliability; creep; fatigue

1. Introduction

The robustness of electronic assemblies is determined by the mechanical integrity of solder joints against various degradation influences. Thermal cycling is one of the environmental effects responsible for degrading the fatigue life of solder joints in real-life applications. Numerous switching on–off cycles for electronics systems as in power cycling and exterior sources of elevated temperature as the heat generated from engines are examples of thermal cycling sources. In thermal cycling, the behavior of solder joints is complicated due to their suffering from several damage mechanisms, including creep, fatigue, and the interaction of both mechanisms. Creep is dominant during dwelling periods, while fatigue is influential between ramps [1,2]. Mainly, joint failure in thermal cycling failure occurs due to the mismatch between the coefficient of thermal expansions between PCB and

components. This would generate cyclic shear stresses on joints as temperature alternating between extremes, named thermomechanical fatigue stress. Microstructure evaluation under thermal cycling includes stress concentration in the defected spots (such as voids) of the microstructure, then recrystallization of Sn grains, followed by intergranular crack growth among grain boundaries. In addition to thermal cycling, drop shock was found to be a vital cause in portable applications such as mobile phones and digital cameras. Researchers [3–7] found that crack initiation in drop tests started from the IMC layer, as it is brittle and considered to be the weakest. This would be enhanced if preceded with few thermal cycles and/or aging due to IMC layer growth caused by thermal aging with time.

Therefore, a joint's initial microstructure has great impact during thermal cycling, including precipitates (Ag₃Sn and Cu₆Sn₅), Sn morphologies, and Sn grain orientations. This is due to the low number of grains in each solder joint: one to three large Sn grains, each with a number of dendrites with the same crystallographic orientation [8–13]. Generally, grain orientation correlates to a joint's reliability, as it plays a vital role in microstructure evolution [14–16] and other phenomena such as electromigration [17]. Moreover, after the reflow process, once the tin (Sn) in solder spheres comes in contact with the copper (Cu) on the solder pads, an intermetallic compound (IMC) is formed, which strengthens the mechanical bond. However, the growth of the IMC layer over time leads to weakening due to its brittle nature. A microstructure study revealed that the component side of the solder junction was where the majority of the cracks originated. There were primarily two sorts of cracks seen: those that go into the bulk solder and those that run along the IMC layer. It was discovered that the crack nearly always started next to the IMC layer, where thermal cycling causes the most stress, and eventually spread into the bulk or along the IMC layer. Other factors such as oxidation and phase change are of significant impact as well [18–22].

SnPb-based alloys show excellent performance in thermal cycling, but the industry switched to lead-free alloys after RoHS prohibited using lead in 2006. Many SAC-based alloys demonstrate competitive performance [23–25]; however, studies are still ongoing to investigate their properties comprehensively. Creep and fatigue are critical mechanical properties of actual solder joints that have been explored by many researchers. Hamasha et al. [26] studied the effect of various testing conditions of varying amplitude and strain rate on the fatigue life of actual joints of SAC105 and SAC305. Results show that SAC305 is more fatigue-resistant compared with SAC105 under varying amplitudes. Sinan et al. [27] investigated the fatigue properties of individual SAC-based doped spheres with various surface finishes. It is found that the higher the Ag content, the superior the fatigue and shear strength obtained. Xu et al. [28] explored the fatigue properties of SAC305 and 105 compared with SnPb alloys under isothermal fatigue conditions and wide strain ranges. SAC305 shows better fatigue properties than SAC105 and SnPb at specific ranges. The effect of surface finish under thermal cycling has been studied extensively. Francy et al. [29] investigated the effect of various surface finishes: OSP, ImAg, and ENIG and alloys under thermal cycling for BGAs and SMRs. ENIG outperformed other surface finishes in the case of BGAs, but with SMRs, OSP and ImAg were slightly better. Similar results were found by [30,31]. Generally, ENIG and ENIPIC were found to perform well in thermal cycling due to their Ni plating layer that blocks the growth of the IMC layer.

Others examined fatigue properties of SAC alloys under various conditions of aging durations and temperatures [28,29], stress amplitudes [30,31], strain ranges [32,33], and shear rates [34]. Many researchers utilized bulk [35,36] and dog-bone [37,38] samples in their work to examine the microstructure evolution [39,40] and fatigue properties of different alloys [40,41] under various conditions. Even though valuable results were obtained, they were not as much as utilizing actual joints due to missing the IMC layer, surface finish, and different microstructure, which impact reliability. Several researchers studied the creep effect under various testing conditions. Fahim et al. [41] examined the evolution of microstructures, including IMC of SAC-based alloys and several surface finishes at various temperatures using nanoindentation testing after aging. Significant degradation in reliability is observed after long-term aging with increasing testing temperature. The

long-term aging of solder junctions at high temperatures causes considerable changes in their microstructure, including a thickening of the intermetallic compound layer (IMC) and coarsening of the precipitates. The mechanical and fatigue characteristics of solder junctions are significantly influenced by their microstructure. Different conditions of aging durations and temperatures were studied [42–46], and similar results were obtained for dominating aging temperature over duration for degradation. Others [28,47,48] explored creep properties and microstructure evolution after several thermal cycles. It is concluded that creep rate and deformation were higher when testing joints after more cycles. Doping is introduced to enhance the properties of the materials by adding small (micro) amounts of certain elements such as Ni, Bi, Cr, etc., to SAC-based alloys. The properties of doped alloys under thermal cycling and iso-thermal cycling have been studied by different researchers [34,42–52]. Doped alloys showed mechanical property improvements depending on the doping element. Various mechanical properties were investigated such as hardness [53], tensile strength [54], and modules of elasticity [55].

There are many models established to predict the fatigue life of several solder materials under thermal cycling with various testing conditions and geometries. Norris and Landzberg [56] were the ones who started early development of the reliability models of SnPb in thermal cycling, considering various temperature and frequency levels. Their model was a modified version of the Coffin–Manson equation. Engelmaier W. [57] studied the fatigue life of SnPb-based CCC joints during power cycling and generated models to predict their life based on the Coffin–Manson model. Most models in the literature were generated based on [51–53] models. Vayman S. et al. [58] created an empirical model for low-tin alloys (SnPb based) under isothermal fatigue conditions including extensive temperature range, hold times, strain ranges, frequencies, and environmental conditions. Salmela O. [59] investigated several acceleration factors for lead-free material under different thermal cycling conditions. He modified the Norris–Landzberg model with a correction factor to compromise for material and geometry. Others established empirical models for lead-free material under thermal cycling [60,61] and isothermal fatigue with aging [62–66].

According to the literature, there is extensive research that investigated the fatigue and creep properties for SnPb-based and lead-free materials. However, limited research has been performed under the combination of both effects in a systematic way. Moreover, comprehensive studies generated models for SnPb and lead-free materials under thermal cycling tests. Nevertheless, there is no study that created a model for actual SAC-based solder joint material under a combination of creep and fatigue. In this study, expanded research of our previous work related to the combined effects of fatigue and creep explored at room temperature [65], and various iso-thermal temperatures [8], is implemented. Moreover, reliability models as a function of dwell time for fatigue life based on Morrow Energy and Coffin–Manson models are generated for SAC305 actual solder joints. These mathematical/empirical models seem to be sophisticated enough to predict life as it was generated according to defined procedures, including identifying the failure mechanism and modes and developing/modifying models based on physics or previous models considering many factors such as temperature, dwell time, etc.

2. Materials and Methods

2.1. Test Vehicle

The test vehicle is a coupon of PCB made of FR-4 glass epoxy with 10 mm × 10 mm × 1 mm dimensions, as shown in Figure 1. Each testing coupon consists of a full array of nine SAC305 solder joints. Each 30 mil-diameter joint is reflowed after being attached to a 22 mil SMD Cu pad. The pitch between joints is 3 mm to assure enough space among joints during testing. OSP is the only surface finish utilized in this work.

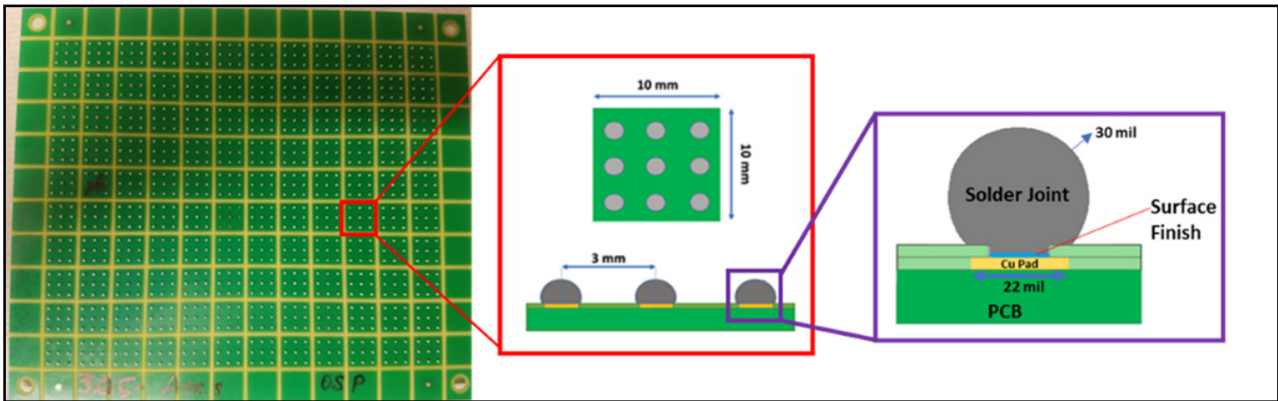


Figure 1. Test Vehicle.

Typical SAC305 solder paste reflow profile is utilized for reflowing the solder joints. The profile starts with a preheating phase to 150–225 °C/200 s, followed by an increase to a peak temperature of 245 °C with less above liquid period than typical SAC305 paste. This is due to the direct exposure of joints to convection heat, unlike assemblies with components. Finally, the temperature is cooled down with a 4 °C/s rate. The whole reflow process is performed within a nitrogen environment. A detailed reflow profile is shown in Figure 2.

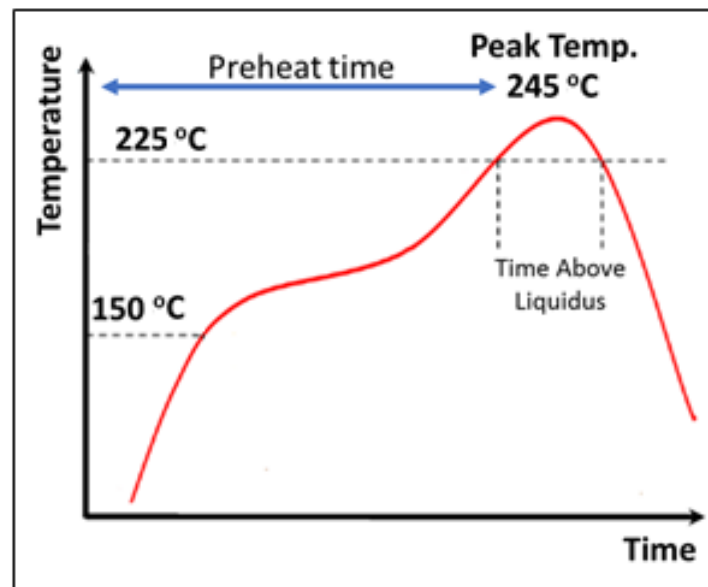


Figure 2. The Reflow profile.

2.2. Experimental Set-Up

Instron 5948 micromechanical tester engaged with a customized fixture is used to implement an accelerated shear fatigue testing on individual solder joints, as shown in Figure 3. The fixture is a circular tip 1 mm in diameter utilized to cycle the joints between stress extremes. The X–Y stage, with the help of a load cell, is used to fit the joints in the middle of the tip and assure the proper tip stand-off range according to the JEDEC standard. A schematic diagram is shown in Figure 4. The displacement and the load are measured by the machine and load cell, respectively. These measurements are recorded continuously by the data acquisition system.

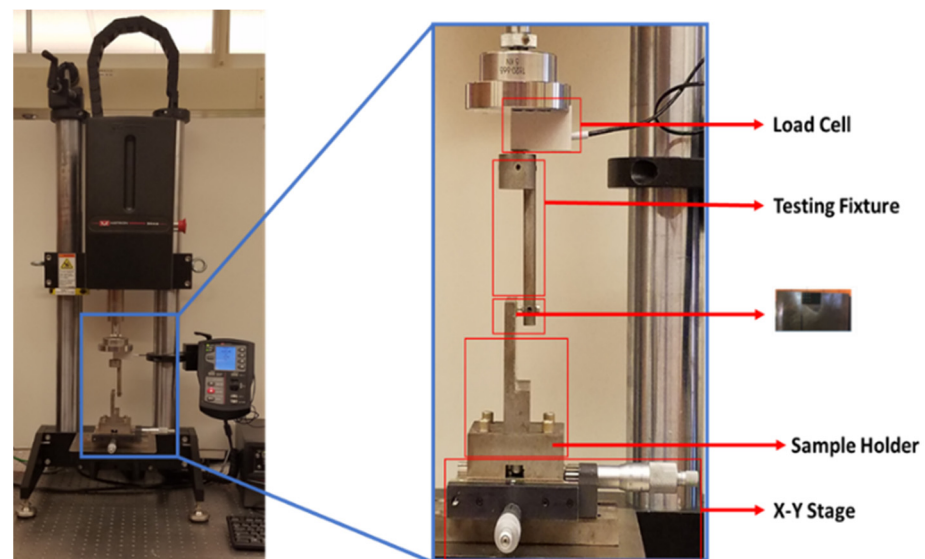


Figure 3. The Instron 5948 Micro-Tester.

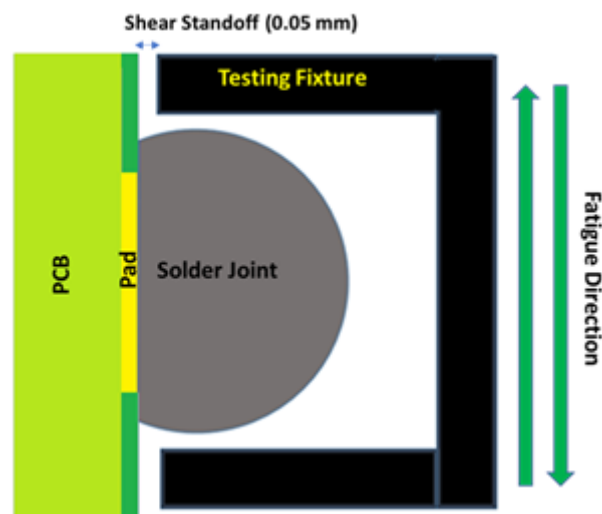


Figure 4. Schematic of a customized testing fixture.

2.3. Test Profile

Two profiles are employed to explore the effects of creep and fatigue in addition to quantifying them. First, a stress-controlled cyclic fatigue test is implemented to examine fatigue effect only, as shown in Figure 5. Cyclic-defined stress is applied at a constant ramp rate of 0.1 mm/s on the solder joint and switched between stress extremes (positive and negative) until complete joint failure (no dwelling conditions). The second profile is of two parts: a stress-controlled followed by a strain-controlled condition, as shown in Figure 6. As soon as the predefined value of stress is reached (stress-controlled) at a positive extreme, the strain is held constant (strain-controlled) for a certain dwelling period. During this part, the material suffers from stress relaxation and/or creep; therefore, it is described as creep–relaxation. Once the dwelling is over, the joint is cycled (switched) to the negative stress extreme with the same conditions of stress and dwelling. The second test is utilized to explore the combined effects of creep and fatigue. The maximum dwelling was 180 s because negligible stress drop (damage) was observed after this duration.

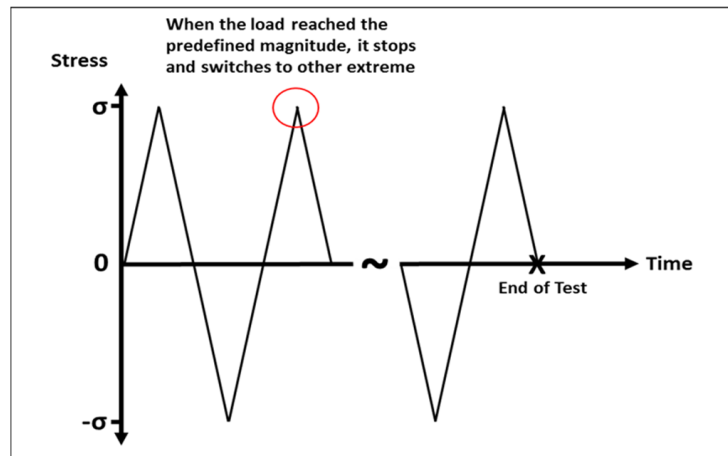


Figure 5. Mechanical fatigue testing profile.

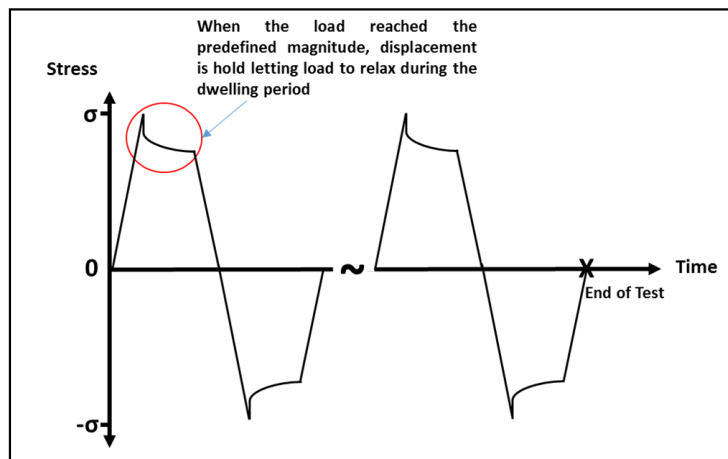


Figure 6. Combined creep-fatigue testing profile.

All experiments were performed at room temperature under several stress magnitudes (16, 20, and 24 MPa) and various dwelling periods (0, 10, 60, and 180 s). A constant ramp rate was employed of 0.1 mm/s for all replicates where seven joints were the sample size for each combination. Picking shear rate is critical in these tests due to viscoplastic behavior on SAC alloys. Faster ramp rate will cause the joints to resist more and does not give it enough time to creep. However, lower rates would cause the creep to be the dominant without allowing any effect for the fatigue. So, the defined shear rate was picked carefully based on previous studies [9–11,20,21] at such types of joints. The test matrix is shown in Table 1.

Table 1. Test Matrix.

Load Amplitude (Mpa)	Fatigue Only Test		Creep-Fatigue Test	
	0 s Dwell	10 s Dwell	60 s Dwell	180 s Dwell
16 MPa	7 samples	7 samples	7 samples	7 samples
20 MPa	7 samples	7 samples	7 samples	7 samples
24 MPa	7 samples	7 samples	7 samples	7 samples

3. Results and Discussions

3.1. Weibull Plots Analysis and Prediction Modeling

3.1.1. Mechanical Fatigue Condition

Weibull Plots

Two parameter Weibull plots are generated for each testing combination to describe the fatigue behavior of solder joints. To demonstrate the degradation in fatigue life or joint reliability, a two-parameter Weibull equation [48] is applied as shown in Equation (1).

$$R(t) = e^{-\left(\frac{t}{\theta}\right)^\beta} \tag{1}$$

where $R(t)$ is the reliability at time t (the probability of not fail), t is the time or number of cycles, θ is the scale parameter or characteristic life, and β is the shape parameter. Figure 7 shows the Weibull plot for joints cycled according to the mechanical fatigue profile (no dwelling) with various stress amplitudes. A significant reduction in joints reliability is observed at higher stress levels. Weibull distribution plots were constructed using Minitab Software for each stress level, considering the maximum likelihood estimation method as the parametric estimation method. The variability of data is low according to the shape (β) parameter values.

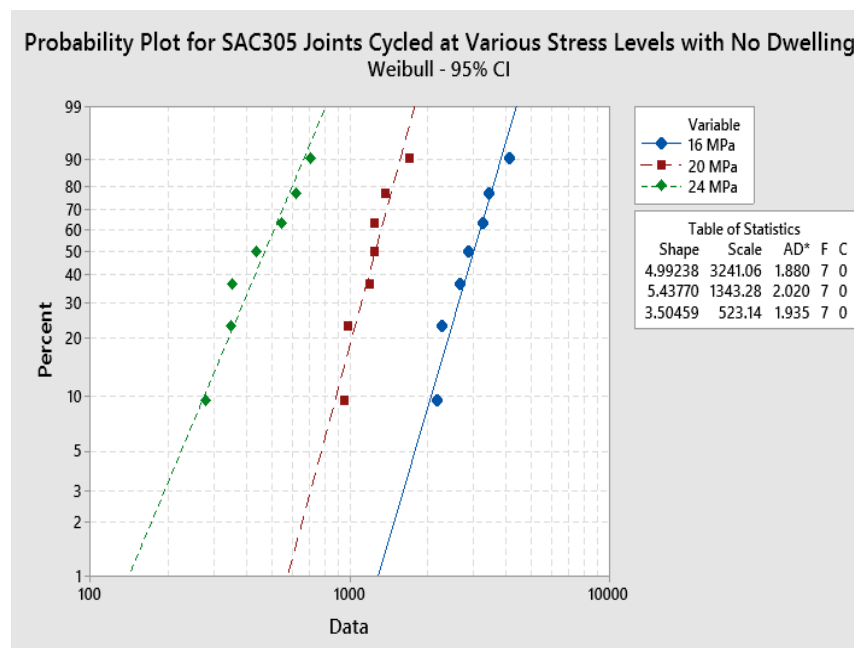


Figure 7. Weibull distributions for SAC305 joints cycled at different stress amplitudes at no dwelling.

Prediction Modeling

The characteristic life and stress amplitude are related according to power equation [48] shown in Equation (2).

$$N_{63} = C \times P^{-n} \tag{2}$$

where N_{63} is the characteristic life, P is the stress magnitude, C , n are material constants. n is called the ductility factor where lower value implies higher ductility. Figure 8 illustrates the fatigue life as a function of stress amplitude. Seven solder joints are cycled until complete failure with each stress level. The fatigue life is reduced drastically at higher stress levels.

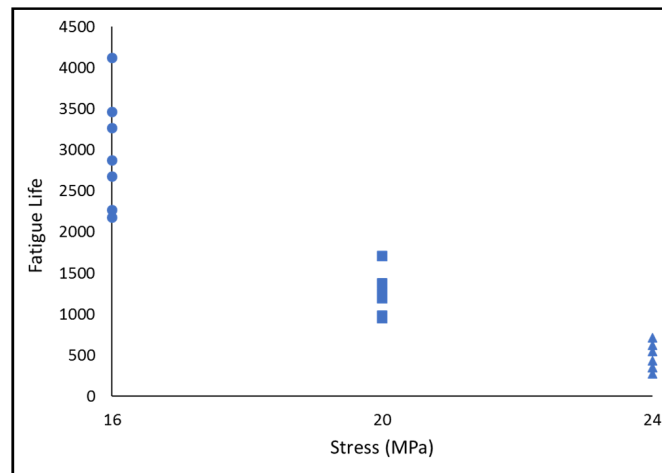


Figure 8. The fatigue life of SAC305 solder joints as a function of stress amplitude.

Characteristic life is a vital parameter to define reliability as a function of stress level according to Equation (1). Therefore, the characteristic life of SAC305 joints as a function of stress amplitude at the “no dwelling” condition is plotted, as shown in Figure 9. Data were fitted to a power equation which was found satisfactory to describe the characteristic life of joints as a function of stress amplitude according to Equation (2). It is concluded that the power value for the generated power equation is -4.34 , which reflects the fatigue ductility exponent coefficient of the material. Moreover, increasing the stress value by a factor of 2 will lead to life reduction by a factor of 19. The ductility index (n) represents the material ductility, where the higher value of n means lower ductility. Similar results were found by others [21,66]. C constant in the stress life equation works as a scale parameter of the relationship between the fatigue life and the stress level, and n coefficient provides the shape of this relationship.

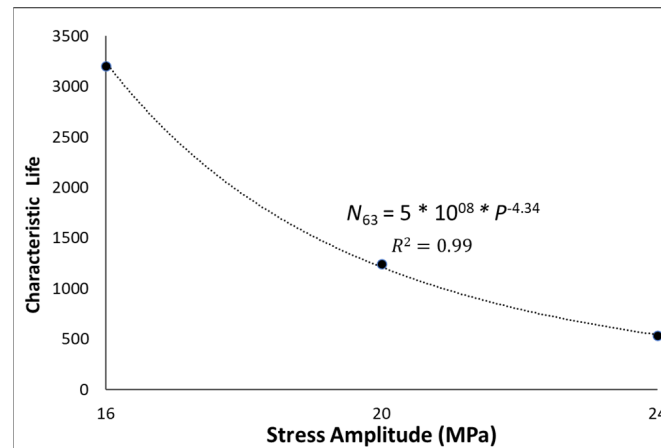


Figure 9. Characteristic life as a function of stress amplitude for SAC305 solder joints at no dwelling.

3.1.2. Dwelling (Creep–Fatigue) Condition Weibull Plots

In order to examine the effects of dwelling on the fatigue life of the solder joints at different stress conditions, individual solder joints were tested at amplitudes of 16, 20, and 24 MPa with different dwell times of 0, 10, 60, and 180 s at 25 °C. The shape and scale parameters of the Weibull distribution were obtained for all combinations. In Figure 10, the Weibull plots for 10 s of dwelling level are generated. At certain dwelling times, increasing the stress amplitude leads to substantial fatigue life reduction. The same trend is found for other dwelling periods of 60 and 180 s. Moreover, at a certain stress level, the fatigue

life is decreased extremely with dwellings of 10 s. Life continues to decrease with longer dwellings but in a smaller amount, as shown in Figure 11. Based on the preliminary life data analysis, only one data point was found as an outlier for the solder joints that were cycled at the 16 MPa stress level with a 180 s dwell time. This data point was eliminated from the reliability analysis. In Figure 12, characteristic life as a function of dwell time for various stress amplitudes is plotted. Creep effect (due to dwelling) was found to be substantial. There are some results for less life of lower stress and higher dwelling conditions than ones cycled with higher stress and shorter dwellings.

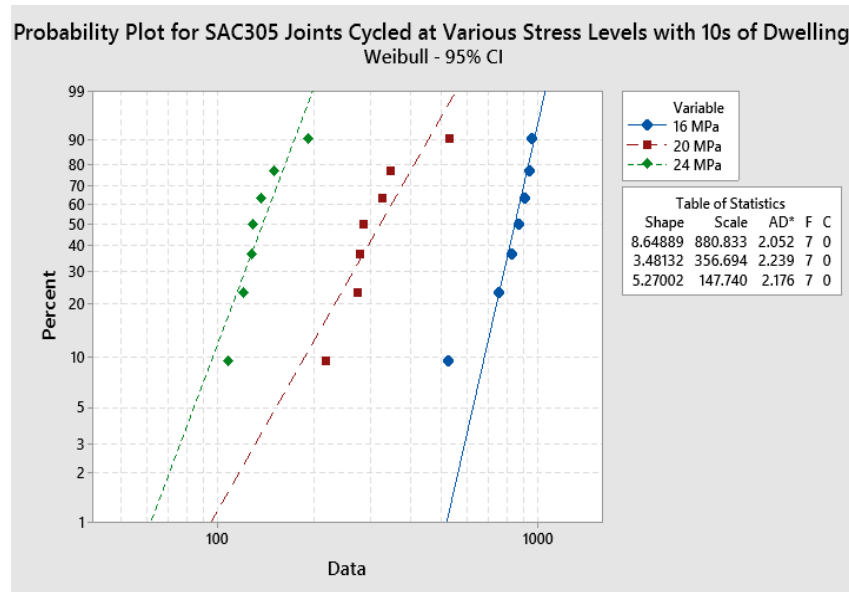


Figure 10. Weibull distributions for SAC305 joints cycled at different stress amplitudes at 10 s dwelling.

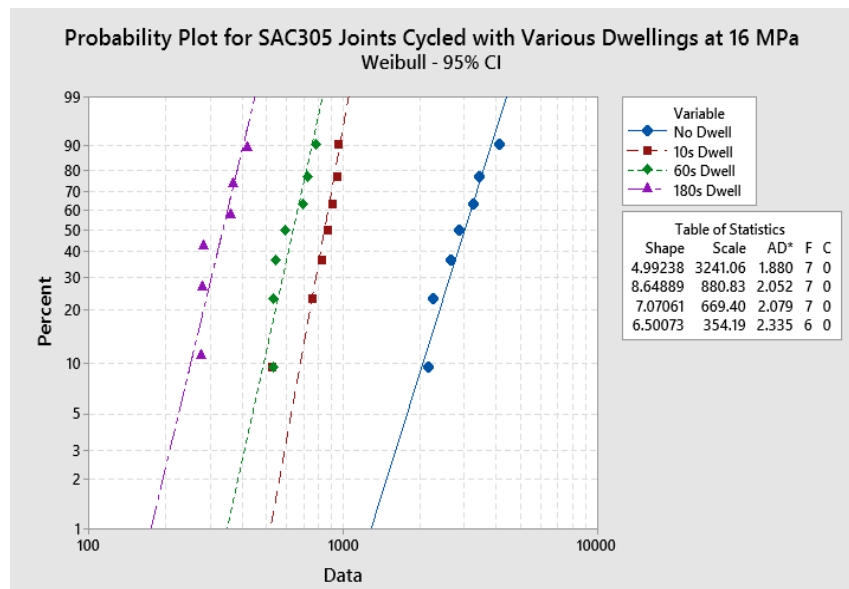


Figure 11. Weibull distributions for SAC305 joints cycled at different dwellings with 16 MPa stress level.

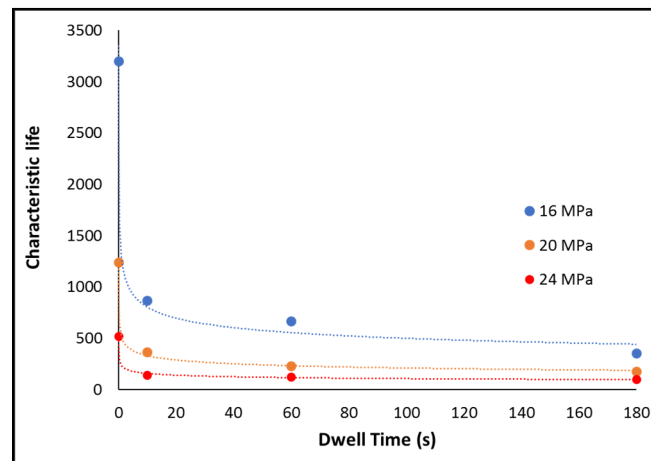


Figure 12. Characteristic life as a function of dwell time for SAC305 solder joints cycled with various stress levels.

Prediction Modeling

To characterize the reliability model as a function of dwelling, the relationship between characteristic life and stress amplitudes for joints cycled with various dwellings are plotted as shown in Figure 13, where data are fitted to power equations for each dwelling period. A decreasing trend for the power value (the material ductility exponent) is identified when the dwell time is increased. However, the constant C was observed to decrease with dwelling. The R-square values are above 99% for all fitting lines.

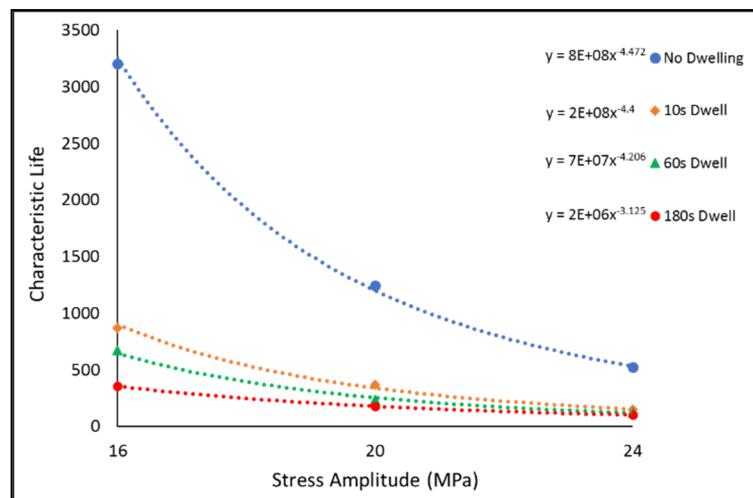


Figure 13. Characteristic life as a function of stress amplitude for SAC305 solder joints at various dwelling times.

To predict the reliability as a function of dwell time and stress amplitude, the correlation between n and C values as a function of dwell time (t_d) must be identified. The correlations to predict the power values of n and C value as a function of dwell time are shown in Figures 14 and 15. From Equation (2), the characteristic life is predicted as a function of stress amplitude and dwell time as shown in Equation (3).

$$N_{63} = 5 \times 10^8 \times e^{(-0.03t_d)} \times P^{(-0.0075t_d+4.5188)} \tag{3}$$

where N_{63} is the characteristic life, P is the stress amplitude, and t_d is the dwell time. To find out the general reliability model of solder joints as a function of dwell time, parameters in Equation (1) must be determined. In our case, there is no observed trend for the shape

parameter of the Weibull plot at different dwell times and stress amplitudes. The shape parameter values were found between 3.5 and 14 with an average of 6.66. For the scale parameter (θ); the finding of characteristic life from Equation (3) is substituted in Equation (1). As a result, the general reliability model as a function of dwell time is established as shown in Equation (4).

$$R(t) = e^{-\left(\frac{t}{5 \times 10^8 \times e^{(-0.03 \times t_d)} \times P^{(0.0075 \times t_d + 4.5188)}}\right)^{6.66}} \quad (4)$$

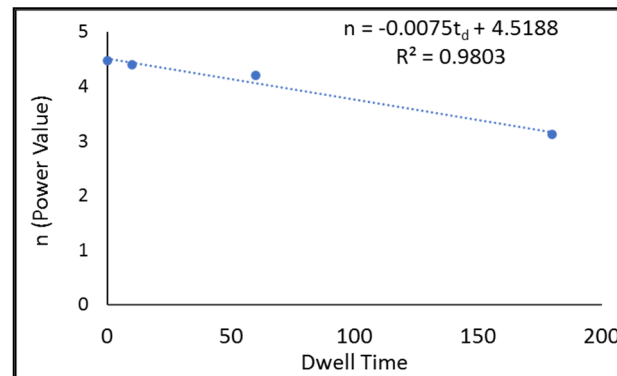


Figure 14. Power value (n) as a function of dwell time.

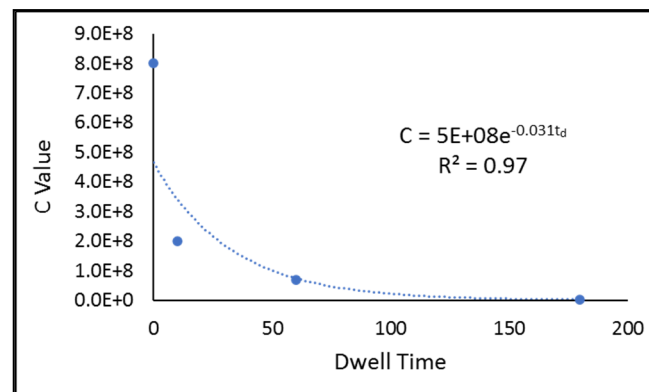


Figure 15. Constant (C) as a function of dwell time.

3.2. Stress–Strain Analysis

Hysteresis loops or stress–strain loops are essential to determine the damage parameters for each cycle represented by the inelastic work and plastic strain per cycle. These parameters are directly related to the accumulated damage. The loop area represents the inelastic (damage) work per cycle, where its width along the x -axis represents plastic strain. Figure 16 shows the average hysteresis loops for joints cycled with various stress levels at no dwelling. Both inelastic work (area inside the loop) and the plastic strain are obviously increased with higher stress amplitude. In Figure 17, average hysteresis loops are generated for 10 s of dwelling periods. At a specific dwelling, the same trend is observed; the hysteresis loop is enlarged drastically at higher stress levels. Moreover, more stress–relaxation is noticed with higher stress magnitudes. The enlargement of hysteresis loops is due to a massive increase in accumulated damaged work due to the creep effect in addition to fatigue damage. Consequently, evolution in hysteresis loops is generated for various dwelling times at certain stress levels of 24 MPa, as shown in Figure 18. Similar behavior is noticed for the plastic strain parameter. The higher stress or more prolonged dwelling would cause more plastic strain to be accumulated at a particular dwelling or stress levels, respectively.

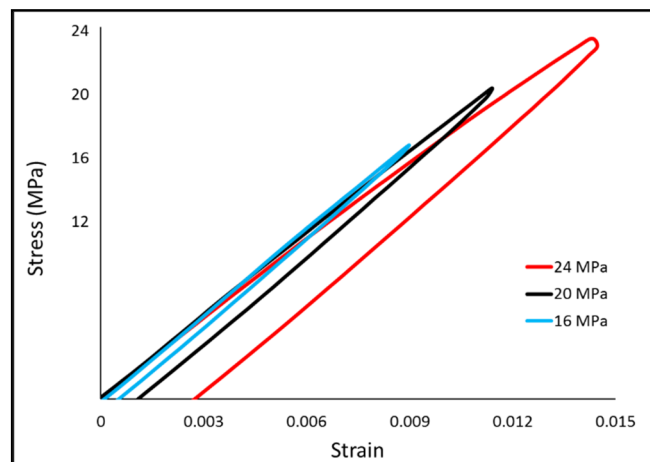


Figure 16. The hysteresis loops for SAC305 joints cycled with different stress amplitudes at no dwelling.

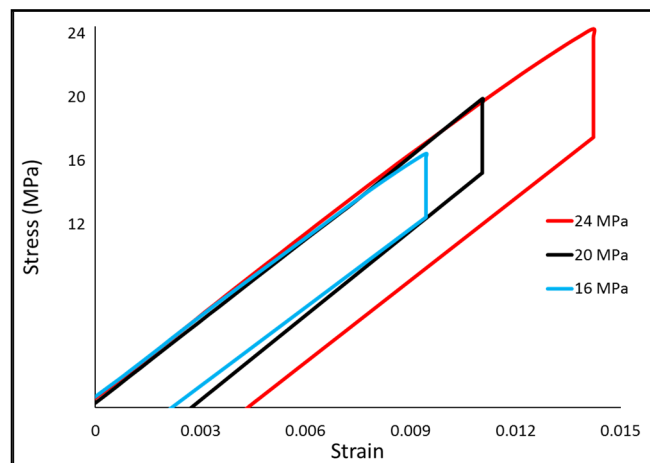


Figure 17. The hysteresis loops for SAC305 joints cycled with different stress amplitudes at 10 s dwelling.

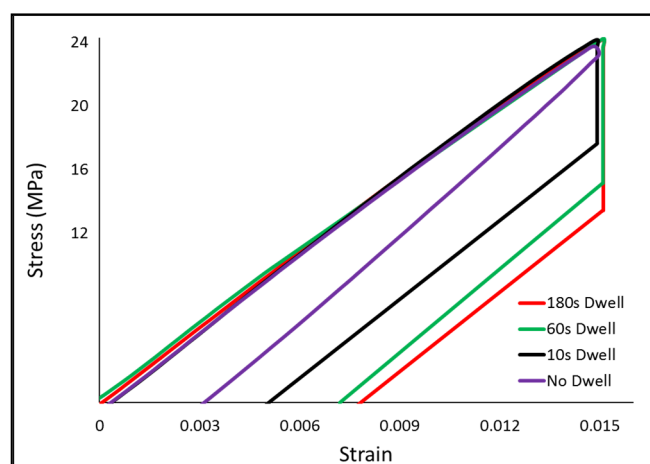


Figure 18. The hysteresis loops for SAC305 joints cycled at various dwellings with 24 MPa stress level.

The evolution in the hysteresis loop is directly related to the damage parameters, inelastic work, and plastic strain per cycle. Therefore, it is essential to examine the progression of such parameters during the joint lifetime to explain the evolvement of stress–strain loops. Figure 19 represents the typical development of inelastic work during the joint's life. This would provide an understanding of such behavior. The evolution is divided into three

regions; the first region is the strain hardening, and it lasts for a few cycles. The second region includes the constant or steady-state region, which represents most of the joint's life. The last phase is the crack initiation and propagation. The same behavior is noticed for all combinations of dwellings and stress levels, as shown in Figures 20 and 21.

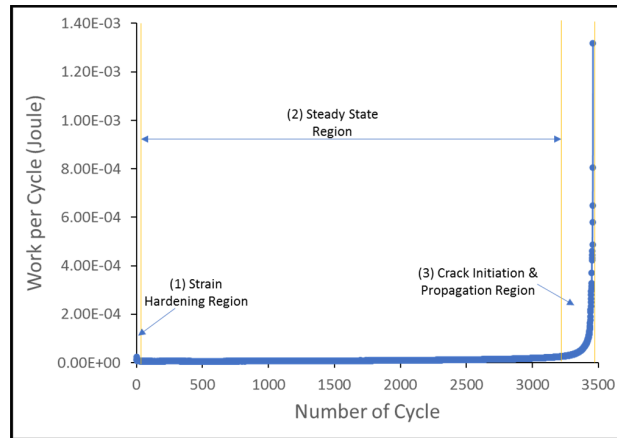


Figure 19. Inelastic work vs. the number of cycles for SAC305 solder joints cycled at 16 MPa stress amplitude until failure.

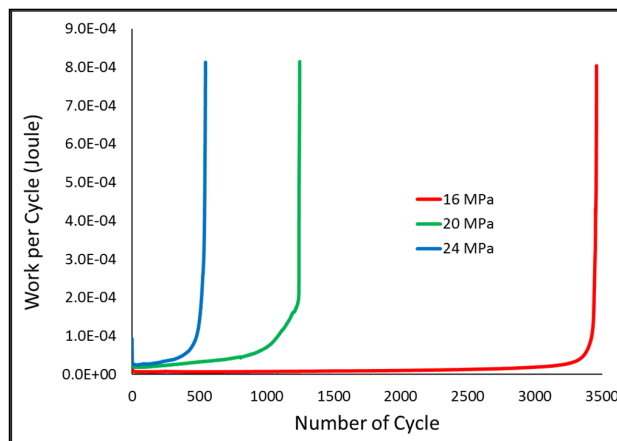


Figure 20. Inelastic work vs. the number of cycles for SAC305 solder joints cycled at various stress amplitudes at no dwelling until failure.

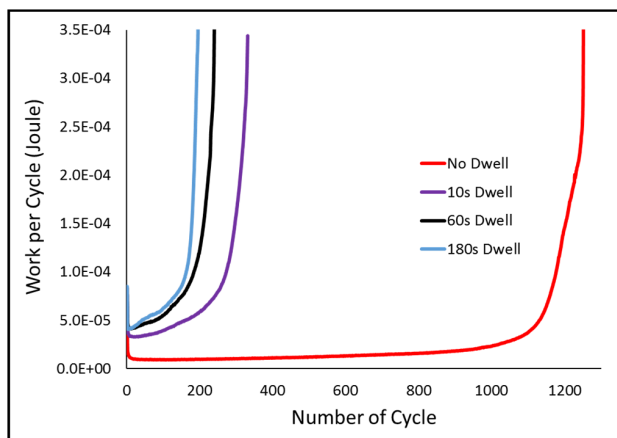


Figure 21. Inelastic work vs. the number of cycles for SAC305 solder joints cycled at 20 MPa stress amplitudes at various dwellings until failure.

3.3. Creep Effect

In this study, the creep effect is demonstrated by evaluating the damaged work per cycle and comparing it for both conditions of no and 10 s of dwelling. At the no dwelling conditions, the damaged work is related to cyclic fatigue only, since the only effect is mechanical fatigue. The creep effect is considered negligible due to the fast ramp rate employed. This would not allow a considerable creep effect to take place between ramps. However, the damage due to creep is dominant during dwelling, and the damage due to fatigue is acquired between ramps in the case of a combined creep–fatigue test. According to the above, it is assumed that inelastic (damaged) work is caused by fatigue only in the cyclic fatigue test with no dwelling, and inelastic (damaged) work due to creep–fatigue is generated due to the combined effects of creep–fatigue at dwelling conditions. Consequently, the damaged work due to creep is determined approximately by subtracting damage due to fatigue only (at no dwelling) from the one generated in the dwelling experiment. Figure 22, for example, shows the hysteresis loops for both conditions of no dwelling (green-colored) and with 10 s of dwelling (yellow-colored) in addition to a bar chart summarizing the damaged work generated for both cases. For more clarification, the damaged work due to fatigue is colored as green in the bar graph, and the damage due to creep is added accordingly for each case with more extended dwelling periods. Results show that work due to creep increases with longer dwelling times, where the related damage on a life reduction basis is reflected obviously. Despite the amount of inelastic work due to creep being almost similar to fatigue in the case of 10 s dwelling, the reflection on life reduction is massive by reducing life by a factor of 3. The same trends for other stress levels with higher damaged work are noticed due to more damaged being created due to higher stress.

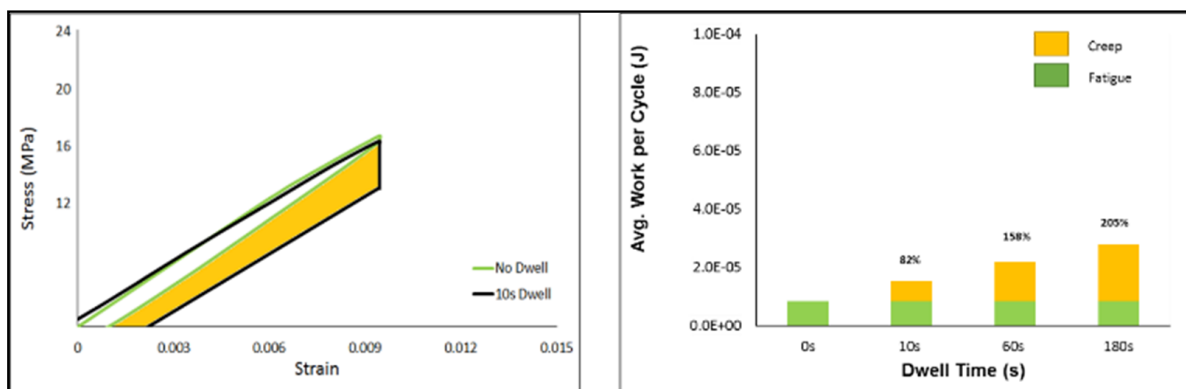


Figure 22. Hysteresis loops (right) with no dwelling and with 10 s dwelling cycled at 16 MPa, and a bar chart (left) for average inelastic work for both cases.

Figure 23 illustrates the average accumulated work until complete failure for SAC305 joints as a function of the dwell times time for different stress levels. For a certain stress level, it is noticed that increasing dwelling periods generates lower accumulated work until complete failure. This can be explained by the smaller amount of cycles observed until complete failure for extended dwellings which are accompanied with less accumulated work. Accumulated work includes other types than damaged or plastic work, which might be work due to friction or generated heat accompanied with each cycle. The trend is different during the dwellings. At no dwelling, 10 s, and 60 s of dwellings, the lower stress level generates more accumulated work than higher stress ones due to the significant additional cycles (accompanied with more accumulated work) observed until complete failure. On the other hand, the non-significant difference in the number of cycles until complete failure at 16 MPa stress level compared with the other stress levels of 20 and 24 MPa causes less accumulated work at 180 s of dwelling. Moreover, the number of cycles until complete failure for 20 and 24 MPa are close together, but more accumulated work is

generated in the case of 24 MPa due to the higher average damage work during the 180 s dwelling. That is why it shows more accumulated damage work in the case of 24 MPa.

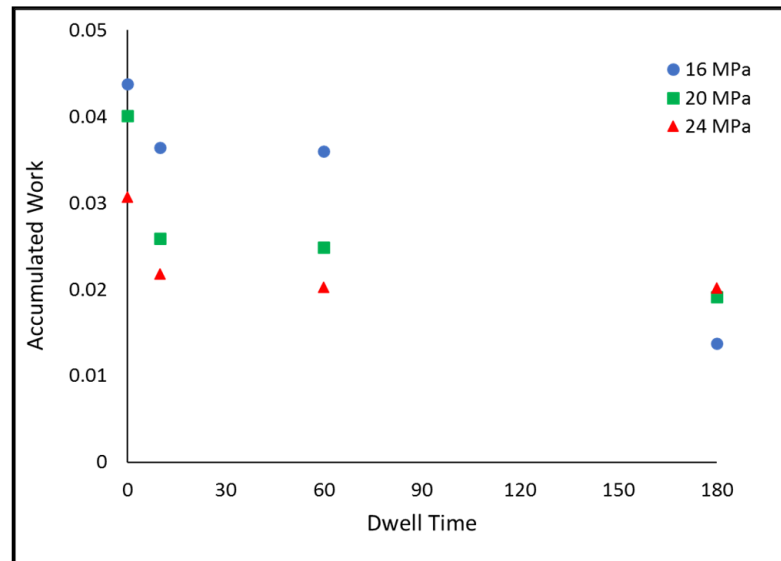


Figure 23. Accumulated work until complete failure vs. dwell time at different stress amplitudes.

Figures 24 and 25 illustrate the average inelastic work per cycle and plastic strain as a function of dwell time, respectively. Both the average work per cycle and the plastic strain were observed to increase with higher stress levels at specific dwellings drastically. This can be explained by more damage accumulating with higher stress levels at fixed dwelling and generating more inelastic work and plastic strain. Moreover, the longer dwelling would produce more inelastic work and plastic strain at a specific stress level. This is due to creep damage accumulated with extended dwellings. However, the creep effect might be substantial on both quantities of inelastic work and plastic strain compared with stress level. In many cases, inelastic work and plastic strain are higher at lower stress levels with longer dwellings than higher stress amplitude with shorter dwell times.

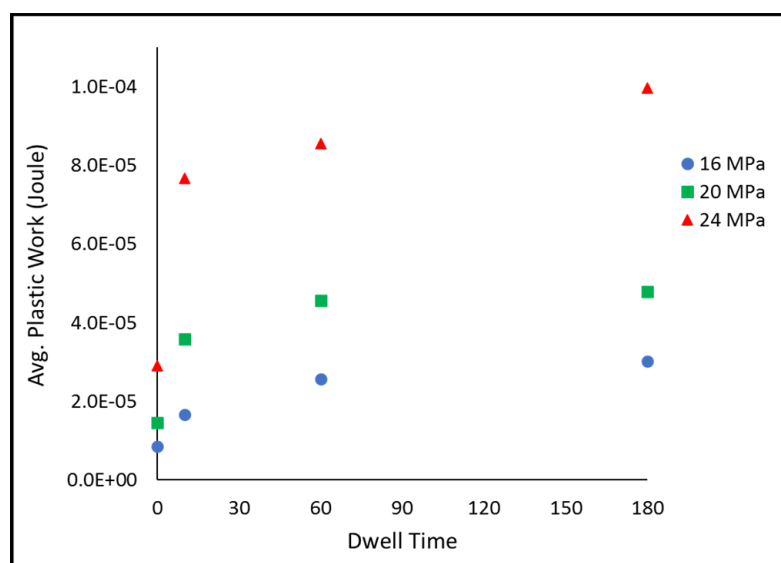


Figure 24. Average work per cycle as a function of dwelling times at various stress levels.

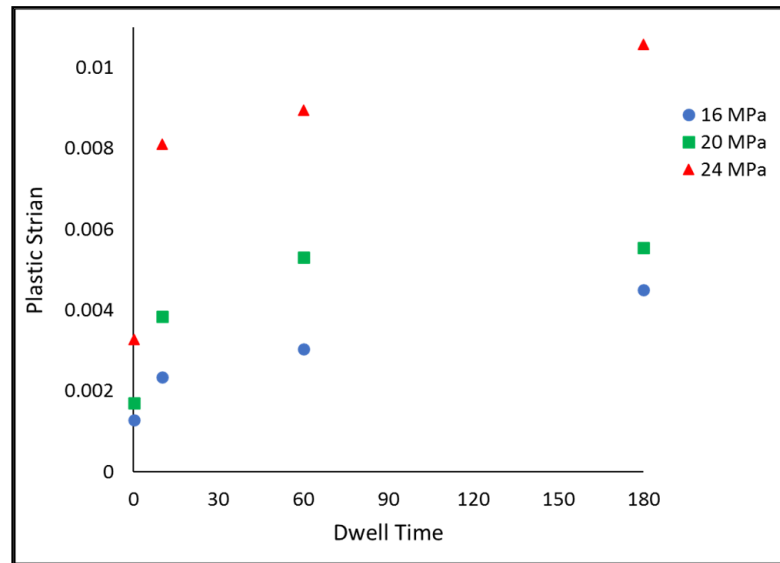


Figure 25. Plastic strain per cycle as a function of dwelling times at various stress levels.

3.4. The Coffin–Manson and Morrow Energy Models

Coffin–Manson Model

Figure 26 describes the plastic strain as a function of dwell time. It is clearly shown that there is a trend of plastic strain as a function of dwell time at various stress amplitudes. With a high *R-square* for all curves, data are fitted to a power equation, so the plastic strains can be predicted as a function of dwell time according to Equation (5).

$$PS = D \times t_d^{0.119} \tag{5}$$

where *PS* is the plastic strain, *D* is constant, and *t_d* is the dwell time. The *D*-value could also be formulated as a function of stress amplitude according to Figure 27. Thus, Equation (6) can be expressed as shown in Equation (6). The dwell time’s impact on the value of the plastic strain is depicted by the *D* coefficient in terms of its magnitude.

$$PS = 0.0003 e^{0.1248 P} \times t_d^{0.119} \tag{6}$$

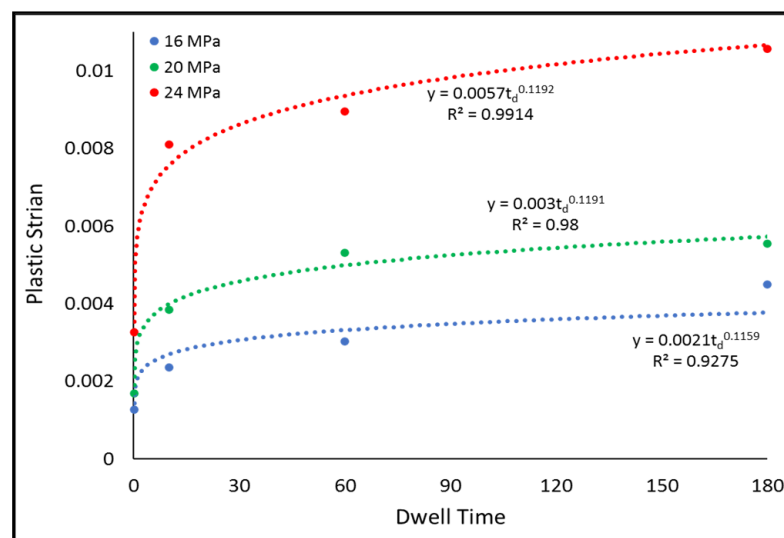


Figure 26. Plastic strain per cycle as a function of dwelling time curves at various stress levels.

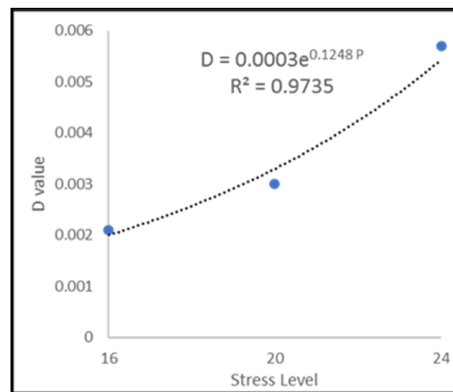


Figure 27. D-value as a function of stress amplitude.

Coffin–Manson is one of the most common models employed for fatigue life prediction as a function of plastic strain. The correlation between fatigue life and plastic strain is illustrated in Equation (7).

$$N_{63} = PS^{\frac{1}{R}} Z^{-\frac{1}{R}} \tag{7}$$

where N_{63} is the characteristic fatigue life, Z is the fatigue ductility coefficient, PS is the plastic strain, and R is the fatigue exponent. Based on the Coffin–Manson equation, the general reliability model as a function of plastic strain could be developed under certain conditions. If there is no clear trend for the coefficient of fatigue ductility (Z) and the fatigue exponent (R) at various dwellings, this implies that dwelling does not affect the Coffin–Manson equation. Moreover, data points for all conditions should have a similar trend (slope) to be fitted to a global Coffin–Manson equation no matter what the dwelling time is. To establish such a model, the characteristic life as a function of plastic strain (Equation (7)) must be obtained. Then, the new equation is substituted in Equation (1) to obtain the reliability model. To examine the model applicability in our case, the above-stated conditions must be checked. Figure 28 demonstrates the characteristic life as a function of plastic strain for various dwelling periods. Data points have the same trend (slope) and could be fitted to a global Coffin–Manson equation. The values for Coffin–Manson equation constants at various dwellings are generated accordingly, as shown in Table 2. It is obviously shown that there is no clear trend in these constants regardless of the dwelling time. This means dwelling has no effect on the Coffin–Manson model, and a general model could be developed. The values of the coefficient of fatigue ductility (Z) and the fatigue exponent (R) for the global equation are 0.19 and 0.646, respectively. Moreover, the global Coffin–Manson model is illustrated in Figure 29.

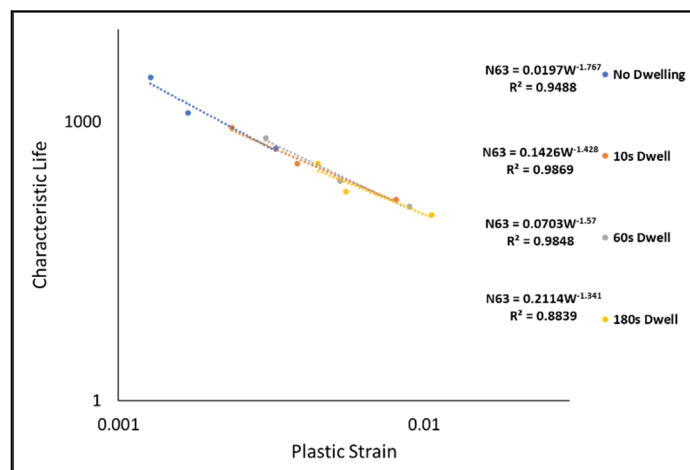
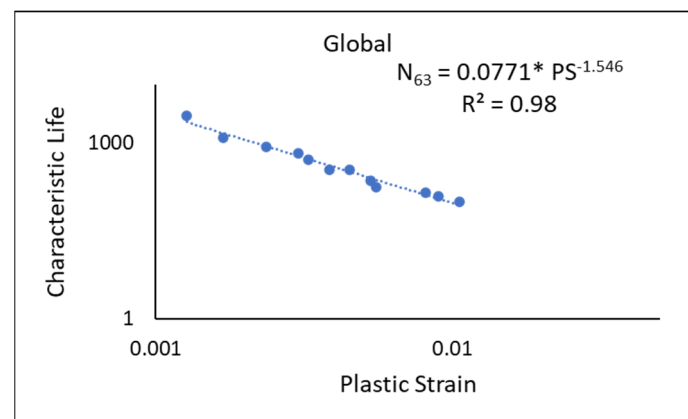


Figure 28. Characteristic life vs. plastic strain for SAC305 joints at various dwelling times on a log–log scale.

Table 2. Fatigue ductility coefficient and fatigue exponent of the Coffin–Manson model.

Dwelling Time	Fatigue Ductility (Z)	The Fatigue Exponent (R)
0	0.108	0.565
10	0.255	0.7
60	0.185	0.636
180	0.313	0.745
Global	0.19	0.646

**Figure 29.** Characteristic life (global Coffin–Manson equation) vs. plastic strain for SAC305 joints at various dwelling times on a log–log scale.

Finally, the characteristic life equation as a function of plastic strain (Equation (8)) must be obtained and substituted in the reliability equation (Equation (1)) to develop the reliability model as a function of plastic strain. The characteristic life as a function of plastic strain is obtained from Figure 29 as shown in Equation (8).

$$N_{63} = 0.0771 \times PS^{-1.546} \quad (8)$$

Substituting Equation (8) in the reliability equation (Equation (1)) and considering the average shape parameter for all combinations as the defined shape parameter, the general reliability model is developed as shown in Equation (9).

$$R(t) = e^{-\left(\frac{t}{0.0771 \times PS^{-1.456}}\right)^{6.66}} \quad (9)$$

where PS is the plastic strain, and t is the number of cycles.

3.5. Morrow Energy Model

Inelastic work is another parameter considered to measure damage, where the Morrow Energy equation is the common related model. Figure 30 illustrates the inelastic work as a function of dwell time for various stress levels. It shows a trend in inelastic work as a function of dwell time at various stress amplitudes. With high R-square for all curves, data are fitted to a power equation, so the inelastic work is predicted as a function of dwell time according to Equation (10)

$$W = H \times t_d^{0.12} \quad (10)$$

where W is the inelastic work, H is constant, and t_d is the dwell time. On the other hand, the H -value could also be formulated as a function of stress amplitude according to Figure 31.

Thus, Equation (10) can be expressed as shown in Equation (11). The H coefficient illustrates the magnitude of the dwell time impact on the value of the inelastic work per cycle.

$$W = (-5.0 \times 10^{-6} \times P - 7 \times 10^{-5}) t_d^{0.12} \tag{11}$$

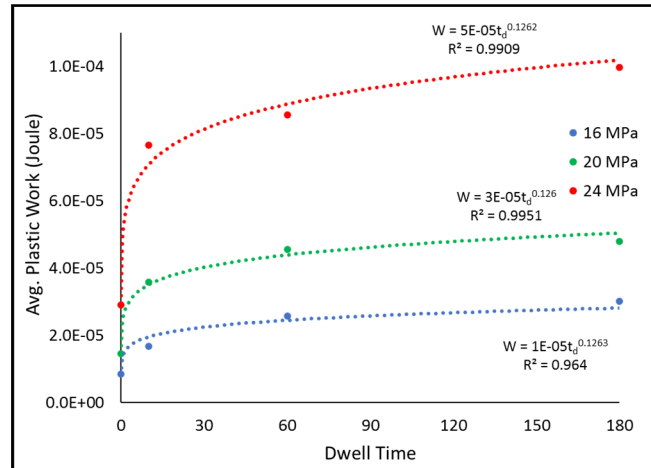


Figure 30. Inelastic work per cycle as a function of dwelling time curves at various stress levels.

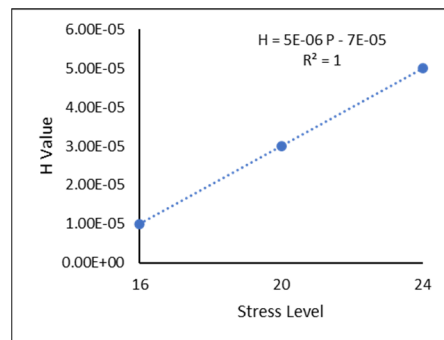


Figure 31. H-value as a function of stress amplitude.

Morrow Energy is a common model used to predict life as a function of inelastic work as shown in Equation (12).

$$N_{63} = G^{\frac{1}{m}} W^{\frac{-1}{m}} \tag{12}$$

where N_{63} is the characteristic fatigue life, G is the fatigue ductility coefficient, W is the inelastic work, and m is the fatigue exponent. In the same way as the Coffin–Manson model, the reliability model as a function of inelastic work based on the Morrow Energy model could be established under similar circumstances defined above. Our data show that fatigue ductility and fatigue exponent have no clear trend at various dwellings, as shown in Figure 32. Furthermore, the data points on a log–log scale demonstrate having a similar trend (slope) and could be fitted to the global Morrow Energy equation. The fatigue ductility and the fatigue exponent constants for all dwellings are specified accordingly, as shown in Table 3. It is obviously shown that there is no clear trend in these constants regardless of the dwelling time. This means dwelling has no effect on the Morrow Energy model, and the global model could be developed. Figure 33 shows the global model for Morrow Energy equation considering that the global constants for fatigue ductility coefficient and fatigue exponent are 0.0025 and 0.737, respectively.

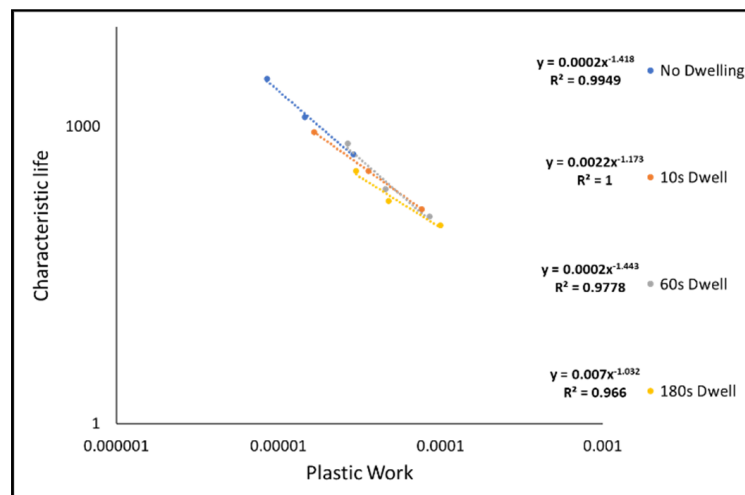


Figure 32. Characteristic life vs. inelastic work for SAC305 joints at various dwelling times on a log–log scale.

Table 3. Fatigue ductility coefficient and fatigue exponent of the Morrow Energy model.

Dwelling Time	Fatigue Ductility (G)	The Fatigue Exponent (m)
0	0.0023	0.713
10	0.0055	0.85
60	0.0028	0.69
180	0.0085	0.96
Global	0.0025	0.737

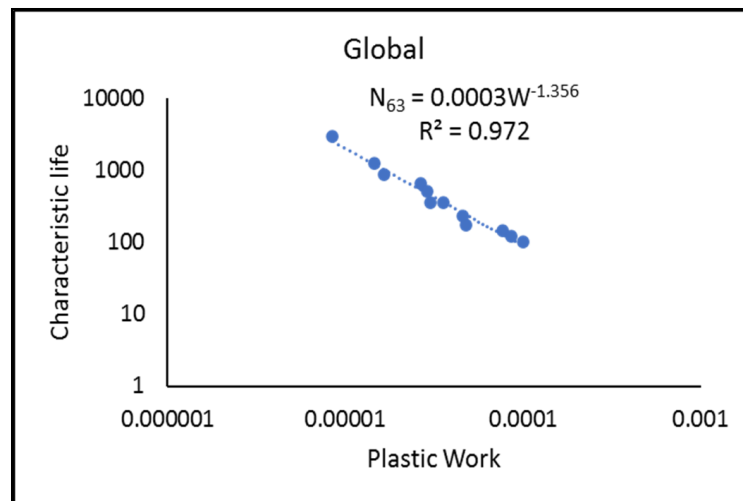


Figure 33. Characteristic life (global Morrow Energy equation) vs. plastic work for SAC305 joints at various dwelling times on a log–log scale.

To generate the reliability model (Equation (1)) as a function of inelastic work, the characteristic life equation as a function of plastic work (Equation (12)) must be attained. Therefore, the characteristic life as a function of plastic work is developed from Figure 33 as shown in Equation (13).

$$N_{63} = 0.0003 W^{-1.356} \tag{13}$$

Finally, substituting Equation (13) in the reliability equation (Equation (1)) and considering the average shape parameter for all combinations as the defined shape parameter, the general reliability model is developed as shown in Equation (14).

$$R(t) = e^{-\left(\frac{t}{0.0003 \times W^{-1.356}}\right)^{6.66}} \quad (14)$$

where W is the plastic work, and t is the number of cycles.

3.6. Microstructure Analysis

The failure mode for samples at room temperature was determined by studying SEM images for tested joints after various dwelling times. This would provide an idea about the effect of dwelling on material evolution under various dwelling periods. Results show that failure is located within the bulk region among all cases of fatigue and creep–fatigue tests as shown in Figure 34.

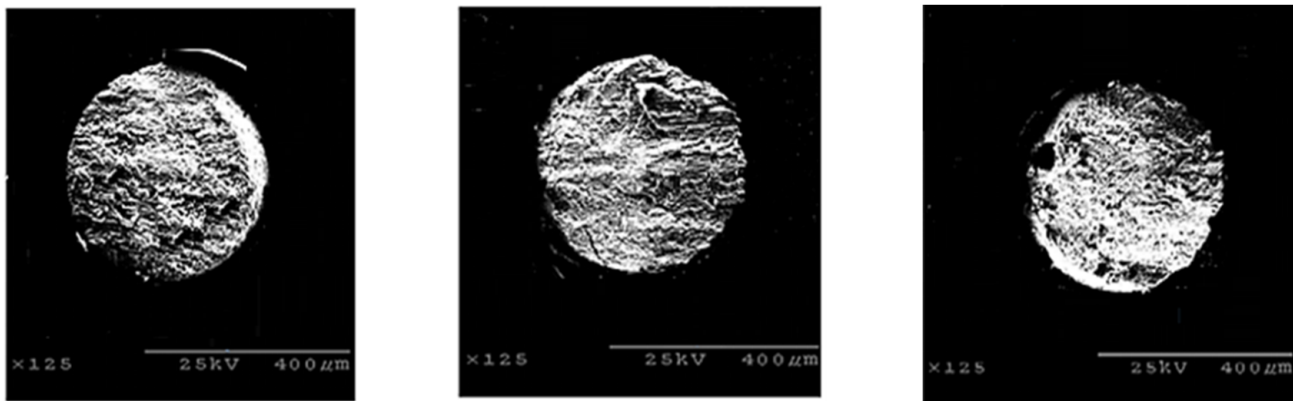


Figure 34. SEM images for tested joints under various dwelling periods compared with no dwelling condition (most left).

4. Conclusions

The damage mechanism under thermal cycling is complicated and not very well understood. Creep and fatigue failure mechanisms related to several factors of dwell time and stress level are detected to have a major degradation effect on fatigue life. It was found that increasing the dwell time and/or the stress magnitude will reduce life. Moreover, at certain stress magnitudes, life is substantially decreased when increasing dwell time. The relation between life and stress amplitude is explored according to the life–stress equation. Results found to fit a power equation for all cases, and empirical models to predict the reliability as a function of dwell time and stress level, were generated accordingly. Furthermore, increasing the dwell time and/or stress level leads to more damage per cycle, which means more dissipated work per cycle and plastic strain. Degradation models were generated as a function of plastic strain and inelastic work per cycle based on Coffin–Manson and Morrow Energy models, respectively.

Author Contributions: Conceptualization, S.H. and M.A.; methodology, R.A.A., S.H. and M.A.; validation, R.A.A. and M.A.; formal analysis, M.A.; investigation, M.A. and M.T.; resources, M.A.; data curation, S.H. and M.A.; writing—original draft preparation, S.H. and M.A.; writing—review and editing, M.T. and S.H.; visualization, S.H.; supervision, S.H.; project administration, R.A.A., M.T. and S.H. All authors have read and agreed to the published version of the manuscript.

Funding: This research received no external funding.

Institutional Review Board Statement: Not applicable.

Informed Consent Statement: Not applicable.

Data Availability Statement: The datasets generated during and/or analyzed during the current study are available from the corresponding author on reasonable request.

Conflicts of Interest: The authors declare no conflict of interest.

References

1. Lau, J.H. Electronics packaging technology update: BGA, CSP, DCA and flip chip. *Circuit World* **1997**, *23*, 22–25. [[CrossRef](#)]
2. Murty, G.S. Stress relaxation in superplastic materials. *J. Mater. Sci.* **1973**, *8*, 611–614. [[CrossRef](#)]
3. Kim, Y.M.; Kim, Y.H. Drop impact reliability of Cu-Zn/Sn-Ag-Cu/Cu-Zn solder joints. In Proceedings of the 2008 International Conference on Electronic Materials and Packaging, Taipei, Taiwan, 22–24 October 2008; IEEE: Piscataway, NJ, USA, 2008; pp. 236–238. [[CrossRef](#)]
4. Waidhas, B.; Proschwitz, J.; Pietryga, C.; Wagner, T.; Keser, B. Study of the board level reliability performance of a large 0.3 mm pitch wafer level package. In Proceedings of the 2019 IEEE 69th Electronic Components and Technology Conference (ECTC), Las Vegas, NV, USA, 28–31 May 2019; IEEE: Piscataway, NJ, USA, 2019; pp. 1159–1164. [[CrossRef](#)]
5. Xu, L.; Pang, J.H. Effect of intermetallic and Kirkendall voids growth on board level drop reliability for SnAgCu lead-free BGA solder joint. In Proceedings of the 56th Electronic Components and Technology Conference, San Diego, CA, USA, 30 May–2 June 2006; IEEE: Piscataway, NJ, USA, 2006; p. 8. [[CrossRef](#)]
6. Lee, J.H.; Kumar, S.; Kim, H.J.; Lee, Y.W.; Moon, J.T. High thermo-mechanical fatigue and drop impact resistant Ni-Bi doped lead free solder. In Proceedings of the 2014 IEEE 64th Electronic Components and Technology Conference (ECTC), Orlando, FL, USA, 27–30 May 2014; IEEE: Piscataway, NJ, USA, 2014; pp. 712–716. [[CrossRef](#)]
7. Xu, L.; Pang, J.H. Effect of thermal and electromigration exposure on solder joint board level drop reliability. In Proceedings of the 2006 8th Electronics Packaging Technology Conference, Singapore, 6–8 December 2006; IEEE: Piscataway, NJ, USA, 2006; pp. 570–575. [[CrossRef](#)]
8. Abueed, M.; Athamenh, R.; Hamasha, S.; Suhling, J.; Lall, P. Effect of Fatigue on Individual SAC305 Solder Joints Reliability at Elevated Temperature. In Proceedings of the 2020 19th IEEE Intersociety Conference on Thermal and Thermomechanical Phenomena in Electronic Systems (ITherm), Orlando, FL, USA, 21–23 July 2020; IEEE: Piscataway, NJ, USA, 2020; pp. 1043–1050. [[CrossRef](#)]
9. Arfaei, B.; Cotts, E. Correlations between the microstructure and fatigue life of near-eutectic Sn-Ag-Cu Pb-free solders. *J. Electron. Mater.* **2009**, *38*, 2617–2627. [[CrossRef](#)]
10. Bieler, T.R.; Jiang, H.; Lehman, L.P.; Kirkpatrick, T.; Cotts, E.J.; Nandagopal, B. Influence of Sn grain size and orientation on the thermomechanical response and reliability of Pb-free solder joints. *IEEE Trans. Compon. Packag. Technol.* **2008**, *31*, 370–381. [[CrossRef](#)]
11. Arfaei, B.; Xing, Y.; Woods, J.; Wolcott, J.; Tumne, P.; Borgesen, P.; Cotts, E. The effect of Sn grain number and orientation on the shear fatigue life of SnAgCu solder joints. In Proceedings of the 2008 58th Electronic Components and Technology Conference, Lake Buena Vista, FL, USA, 27–30 May 2008; IEEE: Piscataway, NJ, USA, 2008; pp. 459–465. [[CrossRef](#)]
12. Bieler, T.R.; Zhou, B.; Blair, L.; Zamiri, A.; Darbandi, P.; Pourboghraat, F.; Lee, T.-K.; Liu, K.-C. The role of elastic and plastic anisotropy of Sn in recrystallization and damage evolution during thermal cycling in SAC305 solder joints. *J. Electron. Mater.* **2012**, *41*, 283–301. [[CrossRef](#)]
13. Lehman, L.P.; Xing, Y.; Bieler, T.R.; Cotts, E.J. Cyclic Twin Nucleation in Tin-Based Solder Alloys. *Acta Mater.* **2010**, *58*, 3546–3556. [[CrossRef](#)]
14. Lee, T.K.; Zhou, B.; Bieler, T.R. Impact of isothermal aging and Sn grain orientation on the long-term reliability of wafer-level chip-scale package Sn–Ag–Cu solder interconnects. *IEEE Trans. Compon. Packag. Manuf. Technol.* **2012**, *2*, 496–501. [[CrossRef](#)]
15. Telang, A.U.; Bieler, T.; Lucas, J.P.; Subramanian, K.N.; Lehman, L.; Xing, Y.; Cotts, E.J. Grain-boundary character and grain growth in bulk tin and bulk lead-free solder alloys. *J. Electro. Mater.* **2004**, *33*, 1412–1423. [[CrossRef](#)]
16. Mondal, D.; Haq, M.A.; Suhling, J.C.; Lall, P. Effects of β -Sn Crystal Orientation on the Deformation Behavior of SAC305 Solder Joints. In Proceedings of the 2022 IEEE 72nd Electronic Components and Technology Conference (ECTC), San Diego, CA, USA, 31 May–3 June 2022; IEEE: Piscataway, NJ, USA, 2022; pp. 1658–1667. [[CrossRef](#)]
17. Fu, X.; Zhou, B.; Yao, R.; En, Y.; Chen, S. Effect of grain orientation and microstructure evolution on electromigration in flip-chip solder joint. In Proceedings of the 2019 IEEE 69th Electronic Components and Technology Conference (ECTC), Las Vegas, NV, USA, 28–31 May 2019; IEEE: Piscataway, NJ, USA, 2019; pp. 1324–1327. [[CrossRef](#)]
18. Etris, S.; Lieb, K.; Sisca, V.; Moore, I.; Batik, A.; Rathore, H.; Yih, R.; Edenfeld, A. Fatigue behavior of solders used in flip-chip technology. *J. Test. Eval.* **1973**, *1*, 170–178. [[CrossRef](#)]
19. Hamasha, S.; Jaradat, Y.; Qasaimeh, A.; Obaidat, M.; Borgesen, P. Assessment of solder joint fatigue life under realistic service conditions. *J. Electron. Mater.* **2014**, *43*, 4472–4484. [[CrossRef](#)]
20. Hamasha, S.; Akkara, F.; Su, S.; Ali, H.; Borgesen, P. Effect of cycling amplitude variations on SnAgCu solder joint fatigue life. *IEEE Trans. Compon. Packag. Manuf. Technol.* **2018**, *8*, 1896–1904. [[CrossRef](#)]

21. Chowdhury, M.; Hoque, M.A.; Fu, N.; Suhling, J.C.; Hamasha, S.; Lall, P. Characterization of material damage and microstructural evolution occurring in lead free solders subjected to cyclic loading. In Proceedings of the 2018 IEEE 68th Electronic Components and Technology Conference (ECTC), San Diego, CA, USA, 29 May–1 June 2018; IEEE: Piscataway, NJ, USA, 2018; pp. 865–874. [[CrossRef](#)]
22. Su, S.; Jian, M.; Wei, X.; Akkara, F.J.; Hamasha, S.; Suhling, J.; Lall, P. Effect of Surface Finish on the Fatigue Behavior of Bi-based Solder Joints. In Proceedings of the 2019 18th IEEE Intersociety Conference on Thermal and Thermomechanical Phenomena in Electronic Systems (ITherm), Las Vegas, NV, USA, 28–31 May 2019; IEEE: Piscataway, NJ, USA, 2019; pp. 1155–1159. [[CrossRef](#)]
23. Kim, K.S.; Huh, S.H.; Suganuma, K. Effects of intermetallic compounds on properties of Sn–Ag–Cu lead-free soldered joints. *J. Alloy. Compd.* **2003**, *352*, 226–236. [[CrossRef](#)]
24. Yoon, J.W.; Kim, S.W.; Jung, S.B. IMC morphology, interfacial reaction and joint reliability of Pb-free Sn–Ag–Cu solder on electrolytic Ni BGA substrate. *J. Alloy. Compd.* **2005**, *392*, 247–252. [[CrossRef](#)]
25. Yu, D.Q.; Wang, L. The growth and roughness evolution of intermetallic compounds of Sn–Ag–Cu/Cu interface during soldering reaction. *J. Alloy. Compd.* **2008**, *458*, 542–547. [[CrossRef](#)]
26. Hamasha, S.D.; Borgesen, P. Effects of strain rate and amplitude variations on solder joint fatigue life in isothermal cycling. *J. Electron. Packag.* **2016**, *138*, 021002. [[CrossRef](#)]
27. Su, S.; Akkara, F.J.; Abueed, M.; Jian, M.; Hamasha, S.; Suhling, J.; Lall, P. Fatigue properties of lead-free doped solder joints. In Proceedings of the 2018 17th IEEE Intersociety Conference on Thermal and Thermomechanical Phenomena in Electronic Systems (ITherm), San Diego, CA, USA, 29 May–1 June 2018; IEEE: Piscataway, NJ, USA, 2018; pp. 1243–1248. [[CrossRef](#)]
28. Xu, H.; Lee, T.K.; Kim, C.U. Fatigue properties of lead-free solder joints in electronic packaging assembly investigated by isothermal cyclic shear fatigue. In Proceedings of the 2014 IEEE 64th Electronic Components and Technology Conference (ECTC), Orlando, FL, USA, 27–30 May 2014; IEEE: Piscataway, NJ, USA, 2014; pp. 133–138. [[CrossRef](#)]
29. Akkara, F.J.; Zhao, C.; Ahmed, S.; Abueed, M.; Su, S.; Hamasha, S.D.; Suhling, J.; Lall, P. Thermal cycling reliability of newly developed lead-free solders for harsh environments. In Proceedings of the SMTA International, Rosemont, IL, USA, 22–26 September 2019.
30. Hamasha, S.; Akkara, F.; Abueed, M.; Rababah, M.; Zhao, C.; Su, S.; Suhling, J.; Evans, J. Effect of Surface Finish and High Bi Solder Alloy on Component Reliability in Thermal Cycling. In Proceedings of the 2018 IEEE 68th Electronic Components and Technology Conference (ECTC), San Diego, CA, USA, 29 May–1 June 2018; pp. 2032–2040. [[CrossRef](#)]
31. Coyle, R.; Parker, R.; Longgood, S.; Sweatman, K.; Howell, K.; Arfaei, B. iNEMI Pb-Free Alloy Characterization Project Report: Part VI-The Effect of Component Surface Finishes and Solder Paste Composition on Thermal Fatigue of SN100C Solder Balls. In Proceedings of the SMTA International Conference, Fort Worth, TX, USA, 13–17 October 2013.
32. Al Athamneh, R.; Abueed, M.; Hani, D.B.; Hamasha, S.D. Effect of aging on SAC 305 solder joints reliability in accelerated fatigue shear test. In Proceedings of the SMTA International Conference, Rosemont, IL, USA, 14–18 October 2018.
33. Al Athamneh, R.; Abueed, M.; Hani, D.B.; Su, S.; Hamasha, S.; Suhling, J.; Lall, P. Effect of aging on the fatigue life and shear strength of SAC305 solder joints in actual setting conditions. In Proceedings of the 2019 18th IEEE Intersociety Conference on Thermal and Thermomechanical Phenomena in Electronic Systems (ITherm), Las Vegas, NV, USA, 28–31 May 2019; IEEE: Piscataway, NJ, USA, 2019; pp. 1146–1154. [[CrossRef](#)]
34. Yang, C.; Chan, Y.S.; Lee, S.R.; Ye, Y.; Liu, S. Comparison of thermal fatigue reliability of SnPb and SAC solders under various stress range conditions. In Proceedings of the 2009 International Conference on Electronic Packaging Technology & High Density Packaging, Beijing, China, 10–13 August 2009; IEEE: Piscataway, NJ, USA, 2009; pp. 1119–1123. [[CrossRef](#)]
35. Osterman, M.; Dasgupta, A.; Han, B. A strain range based model for life assessment of Pb-free SAC solder interconnects. In Proceedings of the 56th Electronic Components and Technology Conference, San Diego, CA, USA, 30 May–2 June 2006; IEEE: Piscataway, NJ, USA, 2006; p. 7. [[CrossRef](#)]
36. Dudek, R.; Kaulfersch, E.; Rzepka, S.; Rollig, M.; Michel, B. FEA based reliability prediction for different Sn-based solders subjected to fast shear and fatigue loadings. In Proceedings of the 2008 International Conference on Electronic Packaging Technology & High Density Packaging, Shanghai, China, 28–31 July 2008; IEEE: Piscataway, NJ, USA, 2008; pp. 1–7. [[CrossRef](#)]
37. Hasan, S.M.K.; Fahim, A.; Suhling, J.C.; Hamasha, S.; Lall, P. Evolution of the Mechanical Behavior of Lead Free Solders Exposed to Thermal Cycling. In Proceedings of the 2019 18th IEEE Intersociety Conference on Thermal and Thermomechanical Phenomena in Electronic Systems (ITherm), Las Vegas, NV, USA, 28–31 May 2019; IEEE: Piscataway, NJ, USA, 2019; pp. 1332–1341. [[CrossRef](#)]
38. Fahim, A.; Hasan, K.; Ahmed, S.; Suhling, J.C.; Lall, P. Mechanical Behavior Evolution of SAC305 Lead Free Solder Joints under Thermal Cycling. In Proceedings of the 2019 18th IEEE Intersociety Conference on Thermal and Thermomechanical Phenomena in Electronic Systems (ITherm), Las Vegas, NV, USA, 28–31 May 2019; IEEE: Piscataway, NJ, USA, 2019; pp. 734–744. [[CrossRef](#)]
39. Zhao, X.; Watte, P.; de Vries, H.; van Hees, G. Challenges in Predicting the Solder Interconnect Lifetime of High Power Electronics. In Proceedings of the 2018 19th International Conference on Electronic Packaging Technology (ICEPT), Shanghai, China, 8–11 August 2018; IEEE: Piscataway, NJ, USA, 2018; pp. 1511–1517. [[CrossRef](#)]
40. Kumar, P.M.; Gergely, G.; Horváth, D.K.; Gácsi, Z. Investigating the microstructural and mechanical properties of pure lead-free soldering materials (SAC305 & SAC405). *Powder Metall. Prog.* **2018**, *18*, 49–57. [[CrossRef](#)]
41. Fahim, A.; Hasan, S.K.; Suhling, J.C.; Lall, P. Nanoindentation Testing of SAC305 Solder Joints Subjected to Thermal Cycling Loading. In Proceedings of the International Electronic Packaging Technical Conference and Exhibition, Anaheim, CA, USA, 7–9 October 2019; American Society of Mechanical Engineers: New York, NY, USA, 2019; Volume 59322, p. V001T08A005. [[CrossRef](#)]

42. Pang, J.H.; Low, T.H.; Xiong, B.S.; Luhua, X.; Neo, C.C. Thermal cycling aging effects on Sn–Ag–Cu solder joint microstructure, IMC and strength. *Thin Solid Films* **2004**, *462*, 370–375. [[CrossRef](#)]
43. Fahim, A.; Ahmed, S.; Suhling, J.C.; Lall, P. Mechanical characterization of intermetallic compounds in SAC solder joints at elevated temperatures. In Proceedings of the 2018 17th IEEE Intersociety Conference on Thermal and Thermomechanical Phenomena in Electronic Systems (ITherm), San Diego, CA, USA, 29 May–1 June 2018; IEEE: Piscataway, NJ, USA, 2018; pp. 1081–1090. [[CrossRef](#)]
44. Yin, L.; Meilunas, M.; Arfaei, B.; Wentlent, L.; Borgesen, P. Effect of microstructure evolution on Pb-free solder joint reliability in thermomechanical fatigue. In Proceedings of the 2012 IEEE 62nd Electronic Components and Technology Conference, San Diego, CA, USA, 29 May–1 June 2012; IEEE: Piscataway, NJ, USA, 2012; pp. 493–499. [[CrossRef](#)]
45. Fahim, A.; Ahmed, S.; Chowdhury, M.R.; Suhling, J.C.; Lall, P. High temperature creep response of lead free solders. In Proceedings of the 2016 15th IEEE Intersociety Conference on Thermal and Thermomechanical Phenomena in Electronic Systems (ITherm), Las Vegas, NV, USA, 31 May–3 June 2016; IEEE: Piscataway, NJ, USA, 2016; pp. 1218–1224. [[CrossRef](#)]
46. Teo, J.R. Thermal cycling aging effect on the reliability and morphological evolution of SnAgCu solder joints. *IEEE Trans. Electron. Packag. Manuf.* **2007**, *30*, 279–284. [[CrossRef](#)]
47. Zhang, J.; Hai, Z.; Thirugnanasambandam, S.; Evans, J.L.; Bozack, M.J.; Zhang, Y.; Suhling, J.C. Thermal aging effects on the thermal cycling reliability of lead-free fine pitch packages. *IEEE Trans. Compon. Packag. Manuf. Technol.* **2013**, *3*, 1348–1357. [[CrossRef](#)]
48. Basit, M.M.; Motalab, M.; Suhling, J.C.; Hai, Z.; Evans, J.; Bozack, M.J.; Lall, P. Thermal cycling reliability of aged PBGA assemblies-comparison of Weibull failure data and finite element model predictions. In Proceedings of the 2015 IEEE 65th electronic components and technology conference (ECTC), San Diego, CA, USA, 26–29 May 2015; IEEE: Piscataway, NJ, USA, 2015; pp. 106–117. [[CrossRef](#)]
49. Akkara, F.J.; Zhao, C.; Athamenh, R.; Su, S.; Abueed, M.; Hamasha, S.; Suhling, J.; Lall, P. Effect of solder sphere alloys and surface finishes on the reliability of lead-free solder joints in accelerated thermal cycling. In Proceedings of the 2018 17th IEEE Intersociety Conference on Thermal and Thermomechanical Phenomena in Electronic Systems (ITherm), San Diego, CA, USA, 29 May–1 June 2018; IEEE: Piscataway, NJ, USA, 2018; pp. 1374–1380. [[CrossRef](#)]
50. Yang, L.; Fenglian, S.; Hongwu, Z.; Yang, W. Influence of Ag, Cu and additive Bi elements on the thermal property of low-Ag SAC solder alloys. In Proceedings of the 2011 6th International Forum on Strategic Technology, Harbin, China, 22–24 August 2011; Volume 1, pp. 72–75. [[CrossRef](#)]
51. Akkara, F.J.; Zhao, C.; Gordon, S.; Su, S.; Abueed, M.; Hamasha, S.; Suhling, J.; Lall, P. Effect of Aging on Component Reliability in Harsh Thermal Cycling. In Proceedings of the 2019 18th IEEE Intersociety Conference on Thermal and Thermomechanical Phenomena in Electronic Systems (ITherm), Las Vegas, NV, USA, 28–31 May 2019; IEEE: Piscataway, NJ, USA, 2019; pp. 717–723. [[CrossRef](#)]
52. Akkara, F.J.; Zhao, C.; Su, S.; Hamasha, S.; Suhling, J. Effects of mixing solder sphere alloys with bismuth-based pastes on the component reliability in harsh thermal cycling. In Proceedings of the SMTA International, Rosemont, IL, USA, 14–18 October 2018.
53. Chen, H.; Wang, L.; Han, J.; Li, M.; Liu, H. Microstructure, orientation and damage evolution in SnPb, SnAgCu, and mixed solder interconnects under thermomechanical stress. *Microelectron. Eng.* **2012**, *96*, 82–91. [[CrossRef](#)]
54. Fu, N.; Suhling, J.C.; Hamasha, S.; Lall, P. Evolution of the cyclic stress-strain and constitutive behaviors of SAC305 lead free solder during fatigue testing. In Proceedings of the 2017 16th IEEE Intersociety Conference on Thermal and Thermomechanical Phenomena in Electronic Systems (ITherm), Orlando, FL, USA, 30 May–2 June 2017; IEEE: Piscataway, NJ, USA, 2017; pp. 1353–1360. [[CrossRef](#)]
55. Erinc, M.; Schreurs, P.J.G.; Geers, M.G.D. Intergranular thermal fatigue damage evolution in SnAgCu lead-free solder. *Mech. Mater.* **2008**, *40*, 780–791. [[CrossRef](#)]
56. Norris, K.C.; Landzberg, A.H. Reliability of controlled collapse interconnections. *IBM J. Res. Dev.* **1969**, *13*, 266–271. [[CrossRef](#)]
57. Engelmaier, W. Fatigue life of leadless chip carrier solder joints during power cycling. *IEEE Trans. Compon. Hybrids Manuf. Technol.* **1983**, *6*, 232–237. [[CrossRef](#)]
58. Vayman, S.; Fine, M.E.; Jeannotte, D.A. Isothermal fatigue of low tin lead based solder. *Metall. Trans. A* **1988**, *19*, 1051–1059. [[CrossRef](#)]
59. Salmela, O. Acceleration factors for lead-free solder materials. *IEEE Trans. Compon. Packag. Technol.* **2007**, *30*, 700–707. [[CrossRef](#)]
60. Solomon, H. Fatigue of 60/40 solder. *IEEE Trans. Compon. Hybrids Manuf. Technol.* **1986**, *9*, 423–432. [[CrossRef](#)]
61. Pan, N.; Henshall, G.A.; Billaut, F.; Dai, S.; Strum, M.J.; Benedetto, E.; Rayner, J. An acceleration model for Sn-Ag-Cu solder joint reliability under various thermal cycle conditions. In Proceedings of the SMTAI, Chicago, IL, USA, 25 September 2005; pp. 876–883.
62. Al Athamneh, R.; Hamasha, S. Fatigue behavior of SAC-Bi and SAC305 solder joints with aging. *IEEE Trans. Compon. Packag. Manuf. Technol.* **2019**, *10*, 611–620. [[CrossRef](#)]
63. Motalab, M.; Cai, Z.; Suhling, J.C.; Zhang, J.; Evans, J.L.; Bozack, M.J.; Lall, P. Improved predictions of lead free solder joint reliability that include aging effects. In Proceedings of the 2012 IEEE 62nd Electronic Components and Technology Conference, San Diego, CA, USA, 29 May–1 June 2012; IEEE: Piscataway, NJ, USA, 2012; pp. 513–531. [[CrossRef](#)]
64. Al Athamneh, R.; Hani, D.B.; Ali, H.; Hamasha, S. Fatigue life degradation modeling of SnAgCu solder joints after aging. *IEEE Trans. Compon. Packag. Manuf. Technol.* **2020**, *10*, 1175–1184. [[CrossRef](#)]

-
65. Abueed, M.; Alathamneh, R.; Suhling, J.; Lall, P. Effect of Creep And Fatigue on Individual SAC305 Solder Joint Reliability in Iso-Thermal Cycling. In Proceedings of the SMTA International, Rosemont, IL, USA, 22–26 September 2019; pp. 308–314.
 66. Won, Y.; Cho, J.; Agonafer, D.; Asheghi, M.; Goodson, K.E. Fundamental cooling limits for high power density gallium nitride electronics. *IEEE Trans. Compon. Packag. Manuf. Technol.* **2015**, *5*, 737–744. [[CrossRef](#)]